Relative contribution of atmospheric drivers to 'extreme' snowfall over the Amundsen Sea Embayment

Pranab Deb[1,1] and Sai Prabala Swetha Chittella[1,1]

[1]Indian Institute of Technology Kharagpur

November 30, 2022

Abstract

We investigate the atmospheric drivers of extreme precipitation over the Amundsen Sea Embayment (ASE) of West Antarctica using daily output from RACMO2 model and re- analysis data (1979-2016). Overall, 93.7% of days with extreme precipitation at the 2 coastal stations of ASE are associated with the 4 dominant Empirical Orthogonal Function (EOF) modes of geopotential height anomalies (at 850 hPa) over West Antarctica. The second EOF mode, associated with a coupled pattern consisting of Amundsen Sea Low and a blocking high to the east, is the main driver of extreme precipitation over ASE, linked to 44.75% of extreme precipitation days. This is followed by EOF-3 (associated with El Niño Southern Oscillation/PSA-1), EOF-4 (likely associated with more frequent 'atmospheric river' events) and EOF-1 (i.e., Southern Annular mode) with a contribution of 22.16%, 21.1% and 12%, respectively. Extreme precipitation linked to EOF-2 and EOF-4 are more intense (by 2 mm/day) than the rest.

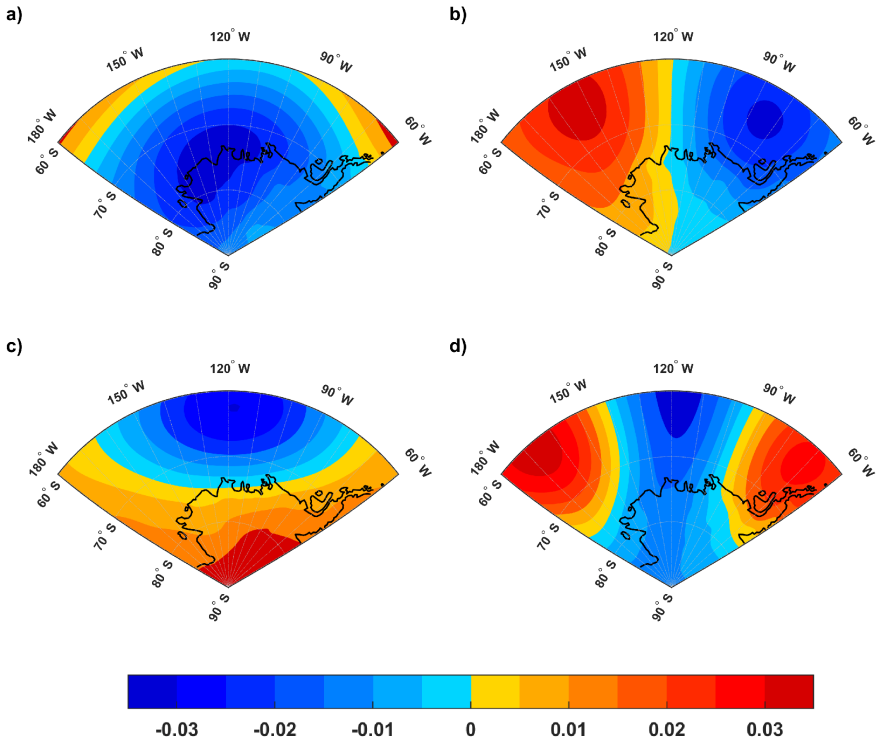

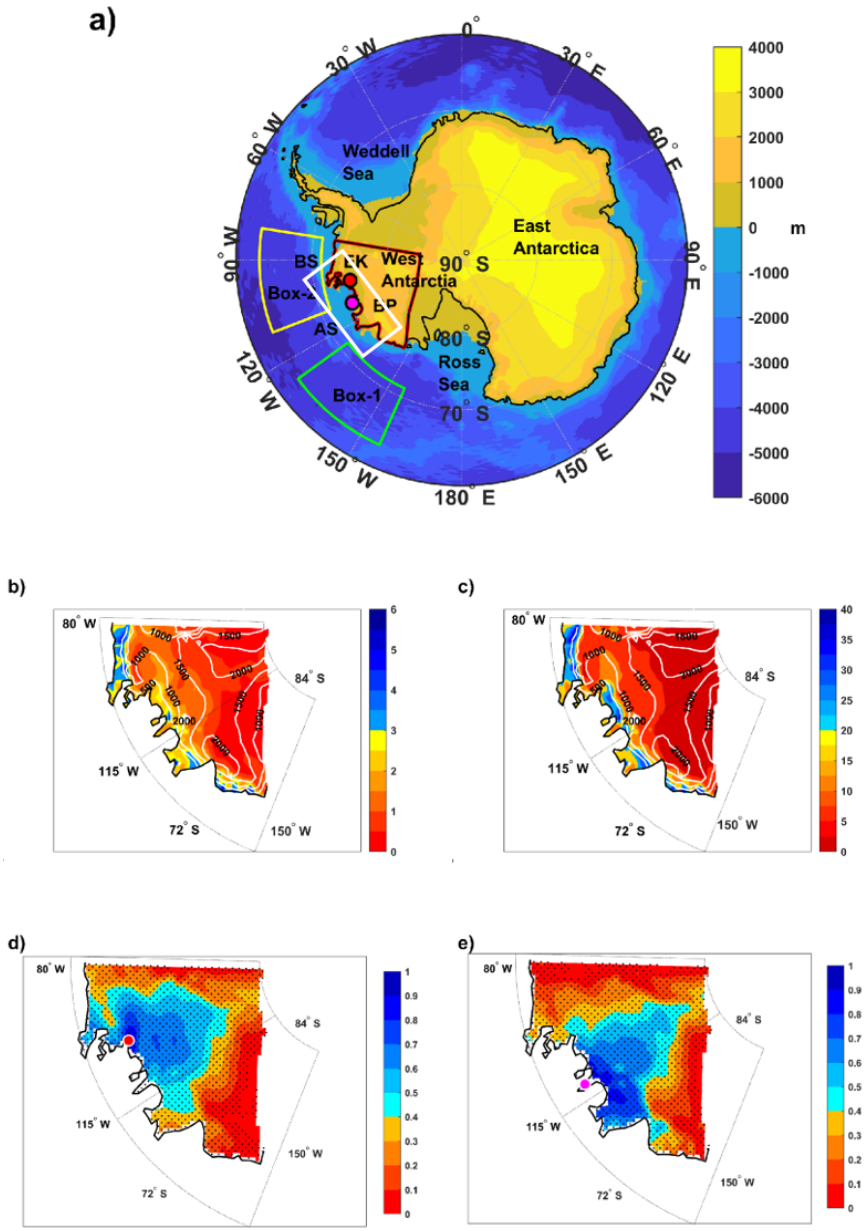

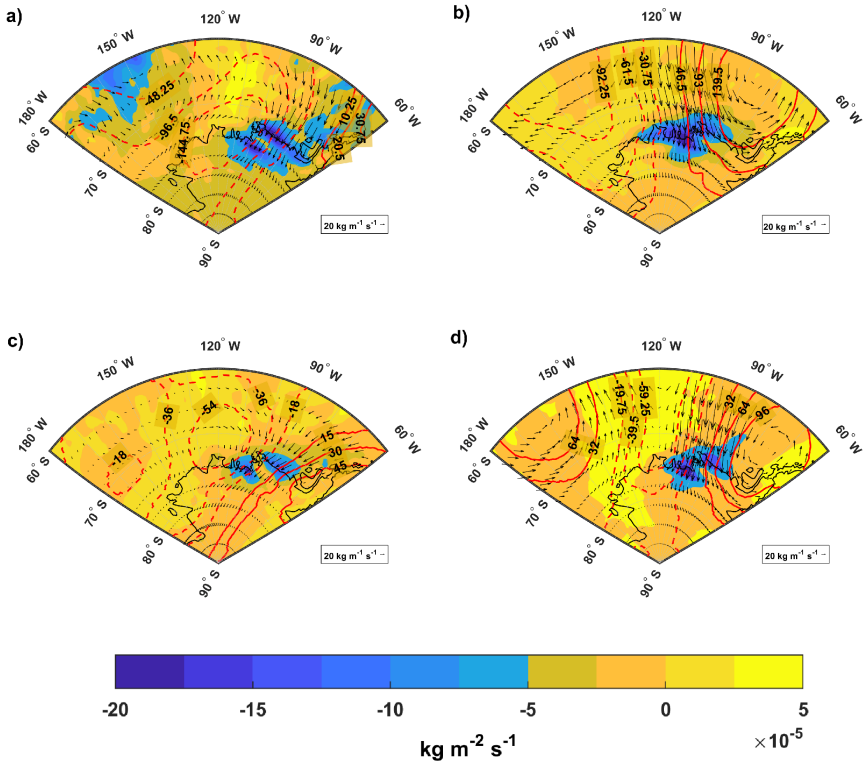

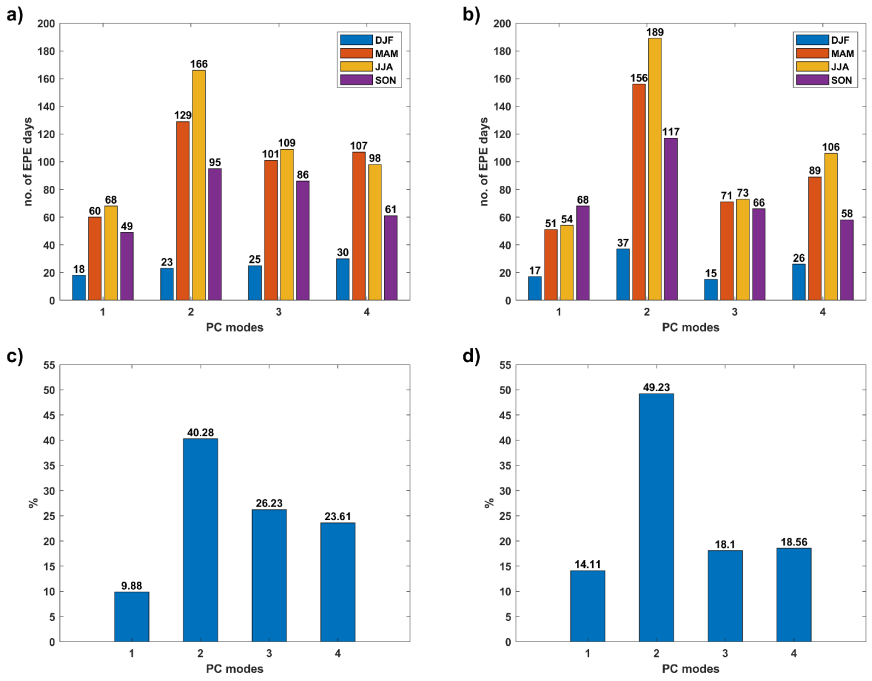

Relative contribution of atmospheric drivers to 'extreme' snowfall over the Amundsen Sea Embayment

[1] **Sai Prabala Swetha Chittella**

[2] **Pranab Deb**

[3] **Jan Melchior van Wessem**

[1,2]Centre for Oceans, Rivers, Atmosphere and Land Sciences, Indian Institute of Technology Kharagpur
[3]Institute for Marine and Atmospheric Research Utrecht, Utrecht University, Utrecht, the Netherlands

Key Points:

- The main drivers of extreme snowfall events over Amundsen Sea Embayment are identified, and their relative contribution is quantified
- A coupled pattern consisting of Amundsen Sea low and a blocking high to the east is the dominant driver of extreme snowfall during 1979-2016
- El Niño Southern Oscillation and 'atmospheric rivers' are also suspected to be linked to several extreme snowfall events over the region

Corresponding author: Pranab Deb, pranab@coral.iitkgp.ac.in

Abstract

We investigate the atmospheric drivers of extreme precipitation over the Amundsen Sea Embayment (ASE) of West Antarctica using daily output from RACMO2 model and reanalysis data (1979-2016). Overall, 93.7% of days with extreme precipitation at the 2 coastal stations of ASE are associated with the 4 dominant Empirical Orthogonal Function (EOF) modes of geopotential height anomalies (at 850 hPa) over West Antarctica. The second EOF mode, associated with a coupled pattern consisting of Amundsen Sea Low and a blocking high to the east, is the main driver of extreme precipitation over ASE, linked to 44.75% of extreme precipitation days. This is followed by EOF-3 (associated with El Niño Southern Oscillation/PSA-1), EOF-4 (likely associated with more frequent 'atmospheric river' events) and EOF-1 (i.e., Southern Annular mode) with a contribution of 22.16%, 21.1% and 12%, respectively. Extreme precipitation linked to EOF-2 and EOF-4 are more intense (by ∼2 mm/day) than the rest.

Plain Language Summary

Snowfall is a key component of the mass balance or 'stability' of the West Antarctic ice sheet. Around 35% of the total precipitation over the Amundsen Sea Embayment of West Antarctica comes from "extreme" snowfall events. We analyse the output from a regional climate model and global reanalysis data to study the seasonal distribution of these extreme events. We identify the atmospheric patterns responsible for these events, and quantify their relative importance. The low pressure system over Amundsen Sea was found to be the dominant driver of these events. Remote forcing due to periodic warming of the tropical Pacific Ocean can also lead to extreme snowfall over the region. Moreover, atmospheric patterns conducive to frequent "atmospheric rivers" events over West Antarctica can cause intense snowfall events in the region.

1 Introduction

The contribution of Antarctic Ice Sheet to the global sea level rise has increased in recent decades, primarily due to ice loss driven by basal melting of ice shelves in West Antarctica (WA) and Antarctic Peninsula (H. Pritchard et al., 2012). The accumulated contribution of WA to sea level rise is 6.9 ± 0.6 mm since 1979 (Rignot et al., 2019). Warmer ocean temperature and incursions of warm circumpolar deep water onto the continental shelf are considered to be the key processes driving the basal melting of WA ice shelves (Vaughan et al., 2001; Mayewski et al., 2009; Summerhayes et al., 2009; Turner et al., 2009).

Antarctic Mass Balance is maintained by accumulation of precipitation, blowing snow and ice loss due to melting, evaporation/sublimation and calving of ice along the coast. The accelerated mass loss from the continent (Rignot et al., 2008; H. D. Pritchard et al., 2009) is partially compensated by snowfall (Zwally et al., 2017; Paolo et al., 2018). As the atmospheric moisture content over Antarctica is low, precipitation in coastal regions is mainly dominated by intense 'high' precipitation events which are highly episodic, and driven by moisture transport from low-latitude areas associated with certain synoptic conditions (Noone & Simmonds, 1998; Sodemann & Stohl, 2009). Generally, these extreme precipitation events (EPEs) are responsible for most of the annual precipitation over coastal Antarctica (Turner et al., 2019). Turner et al. (2009) demonstrated that during 1979–2016, around 70% of the variance in annual precipitation of Antarctica is accounted for by variability in EPEs, with the figure rising to 97% at one location over the Amundsen Sea Embayment (ASE) (83°S, 146°W). Another recent study (Maclennan & Lenaerts, 2021) documents the importance of EPEs over the Thwaites Glacier region in WA, with EPEs accounting for around 60% of the total snowfall.

The spatial variability of different atmospheric and cryospheric parameters in WA is largely

controlled by the large-scale circulation patterns in the southern high latitudes, e.g., the Southern Annular Mode (SAM), the Pacific-South American (PSA1 and PSA2) patterns (Ghil & Mo, 1991; Lau et al., 1994; Kidson, 1988; Deb et al., 2016; G. J. Marshall et al., 2017). The PSA1 pattern is known to be modulated by sea surface temperature anomalies over tropical eastern Pacific Ocean i.e., ENSO variability (Mo & Paegle, 2001). ASE has the strongest teleconnection to ENSO manifested via modifications in the Amundsen Sea Low (ASL) (Deb et al., 2018). PSA2 is a dominant zonal wavenumber-3 pattern in Southern Hemisphere which is also found to be influenced by tropical western Pacific Ocean (M. Raphael, 2004; Clem & Fogt, 2015; Irving & Simmonds, 2015). A coupled atmospheric structure consisting of a blocking high to the west of Antarctic Peninsula and the ASL represents the western branch of the PSA2 pattern (M. Raphael, 2004), and drives a strong meridional flow towards the coastal WA (Deb et al., 2018). G. J. Marshall et al. (2017) showed that polarities of these principal modes of atmospheric circulation control the EPEs over Antarctica. Moreover, "atmospheric rivers" that carry large quantities of moisture from midlatitudes have also been linked to several coastal EPEs in Antarctica (Zhu & Newell, 1998; Gorodetskaya et al., 2014).

The scarcity and uneven distribution of observation records limit our understanding of the fine scale distribution of precipitation, particularly over the coastal regions (Banta et al., 2008; Maclennan & Lenaerts, 2021). Moreover reanalysis products and global climate model simulations are too coarse to capture the complex spatial pattern of topography and related meteorological processes over the region (Orr et al., 2014; Deb et al., 2016). To this end, dynamical downscaling of global reanalysis data using limited-area high-resolution regional atmospheric models (e.g., Giorgi et al. (1994)) has emerged as a useful tool to generate physically consistent temporal and spatial pattern of Antarctic precipitation (J. T. Lenaerts et al., 2013; G. J. Marshall et al., 2017). For example, the performance of the Regional Atmospheric Climate Model (RACMO) has been vetted by two recent studies in capturing the mean and extreme precipitation over Antarctica (Turner et al., 2019; Maclennan & Lenaerts, 2021). These studies have attempted to quantify the variability and contribution of extreme snowfall events over Antarctica (Turner et al., 2019), and to identify the atmospheric drivers of EPEs over the Thwaites glacier region of WA (e.g., Thwaites glacier).

However, no studies exist that quantify the role of dominant atmospheric drivers of EPEs across the ASE, or quantify the seasonal contribution of these drivers to the occurrence of EPEs. Here, we present the intensity and frequency of EPEs over ASE using output from a high-resolution regional climate model (RACMO2). Thereafter, we identify the primary atmospheric drivers of these EPEs, and quantify their relative and seasonal contribution.

2 Data and methods

Daily precipitation flux derived from an Antarctic-wide simulation of RACMO2 (version 2.3,Van Wessem et al. (2014)) during the period from 1979-2016 (January to December) is used to calculate daily precipitation (mm/day). The model uses a horizontal resolution of 27 km and a vertical resolution of 40 levels. The model combines the atmospheric dynamics of the High Resolution Limited Area Model (HIRLAM; Undén et al. (2002)) with the physics package of the European Centre for Medium-Range Weather Forecasts (ECMWF) Integrated Forecast System (IFS). The model is forced by 6-hourly ERA-Interim reanalysis data (Dee et al., 2011), and the interior of domain is set free while the lateral and ocean boundaries are constrained. This model version 2.3 is optimised for polar regions by interactively coupling it to a multilayer snow model (Ettema et al., 2010). A prognostic scheme for snow grain size is used for the calculation of snow albedo (Kuipers Munneke et al., 2011) while the interaction of the near-surface air with drifting snow is simulated by drifting snow scheme (Déry & Yau, 1999; J. Lenaerts et al., 2010).

We define daily EPEs as days during which daily precipitation exceeds the 95^{th} percentile of

daily precipitation values of the whole time series. Empirical Orthogonal Function (EOF) analysis of daily geopotential height anomaly was performed to identify the dominant patterns of atmospheric variability over WA. Spatial patterns of the major EOF modes over the domain encompassing 60°-90°S and 180°-60°W were computed by considering the daily geopotential height anomalies at 850 hPa derived from ERA-Interim reanalysis at a horizontal resolution of 0.75° by 0.75° during 1979-2016. The time series of these EOF modes are called principal components (PCs), are normalised such that their mean is zero and standard deviation is one. Next, the values of the normalised major PCs are extracted for each EPE day. For a particular EPE day, a PC mode is considered to be dominant if the magnitude of the normalised PC is greater than 1 for that day.

Further, moisture divergence and moisture transport data derived from ERA-Interim reanalysis were used to study the atmospheric condition during EPE days. To identify the climatic drivers of the EPEs, several global climate indices were also analysed, e.g., ENSO-Oceanic Niño Index (ONI)(National Weather Service, Climate Prediction Center), Marshall SAM index (G. Marshall, 2018) and ASL index (S. Hosking, 2020). We also define an ASL-lon index, following Deb et al. (2018), as the difference between mean sea level pressure averaged over a box in the western Amundsen Sea region (to the west of 125°W; labeled "Box 1" in Figure-1a) and a box in the Bellingshausen Sea (to the east of 110°W, labeled "Box 2" in Figure-1a). Positive (negative) values of index indicates the eastward (westward) shift of the location of the ASL. This index effectively captures the blocking pattern over WA and the zonal migration of ASL.

3 Results

Spatial distribution of average daily precipitation over WA during 1979-2016 is shown in Figure-1b. Coastal areas with elevation less than 1000 m are associated with higher average precipitation values ($>$ 3 mm/day). The average precipitation values drop down to below 2 mm/day in the inland areas. Over the coastal areas, the mean daily precipitation from EPEs (Figure-1c) is approximately 7 times more than that of average daily precipitation (Figure-1b). Figure-1d shows that the difference of average precipitation from EPEs and average daily precipitation is maximum in the coastal areas ($\sim$ 16–34 mm/day). The mean precipitation from EPEs is much lower (difference $<$ 10 mm/day) further inland when compared to coastal areas. Overall, the total precipitation accumulated for the whole domain (outlined in thick red lines in Figure-1a) is $1.9471*10^4$ Gt out of which the total contribution from EPEs is $6.8523*10^3$ Gt during 1979-2016. Thus, EPEs contribute 35.19% to the total precipitation over the WA domain.

In coastal areas, the mean precipitation linked to EPEs show large values, particularly over the ASE region. In order to capture the characteristics and drivers of EPEs over the ASE, two coastal locations, namely Evans Knoll (EK, red circle in Figure-1e) and Bear Peninsula (BP, magenta circle in Figure-1f), are selected. The time series of average daily precipitation from the two stations are closely related to each another (correlation of 0.7). Moreover, the daily average precipitation at these two stations are significantly correlated to a large portion of the WA, with particularly high correlation over the ASE (Figures-1e and 1f). The precipitation over EK shows the strongest correlation with precipitation over ASE to the east of 115°W (correlation $>$ 0.6), while the precipitation over BP is strongly associated with precipitation over ASE to the west of 95°W (correlation $>$ 0.6). Since, the precipitation at these two locations are representative of precipitation over the entire ASE (and also over a larger WA domain), we focus on these locations instead of area averaged values over ASE.

The frequency distribution and seasonality of EPEs are similar at both the locations (Supplementary Figure-S1 and S2). The maximum number of EPEs occurring in JJA, followed by MAM and SON and significantly less number of EPEs are found in DJF (Supplementary

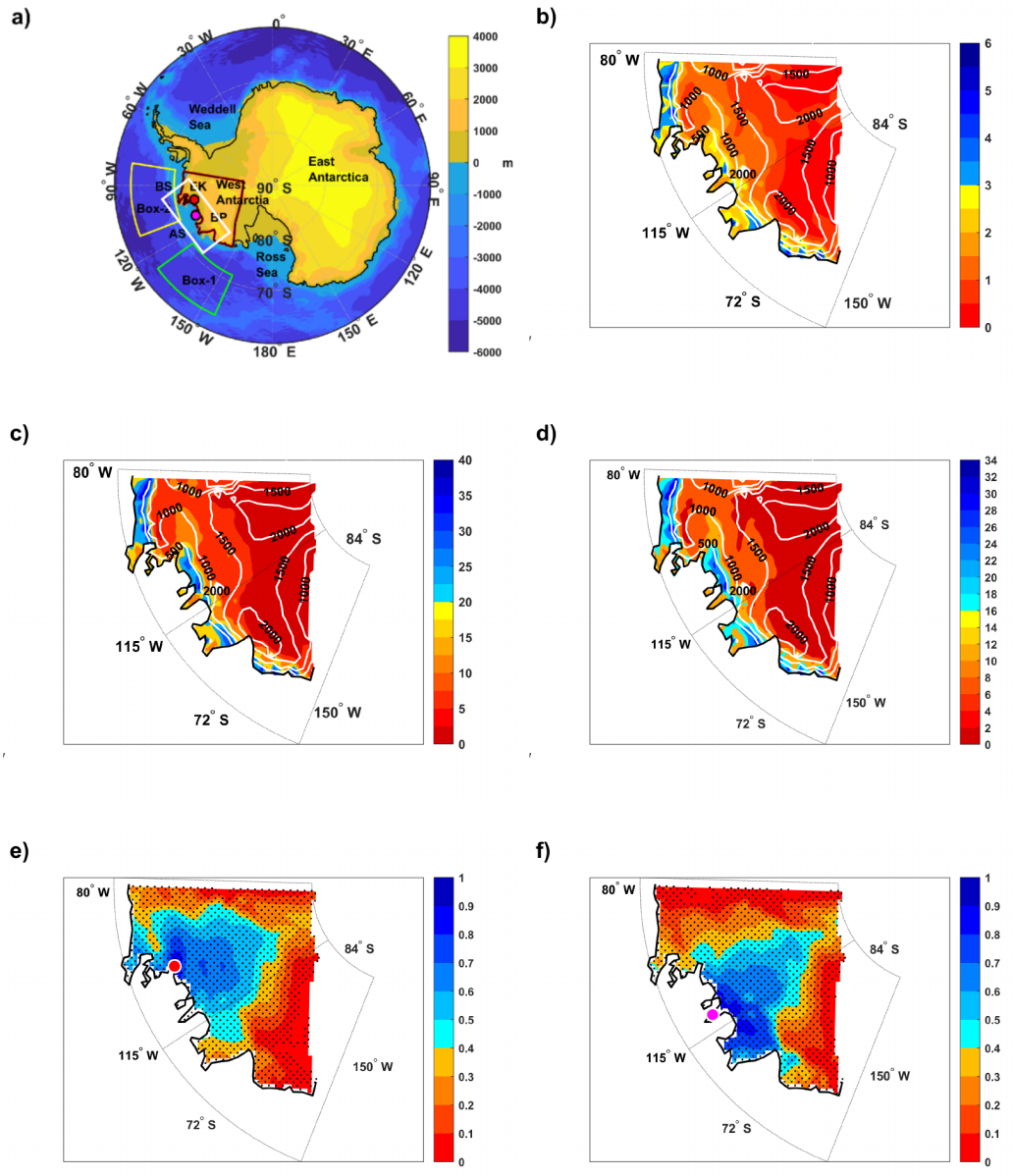

Figure 1. (a) Map of Antarctica with surface elevation in the background (shaded, in m). The Study area outlined in thick red lines. White box is the region of Amundsen Sea Embayment. EK-Evans Knoll, BP-Bear Peninsula, BS- Bellingshausen sea, AS-Amundsen sea, box-1 and box-2 are regions in AS and BS. Spatial distribution of (b) average daily precipitation (mm/day) and (c) average precipitation (mm/day) from all EPEs at each grid of study area for time period 1979-2016.(d) Difference of average precipitation from EPEs and average daily precipitation. Correlation between (e) Evans Knoll and (f) Bear Peninsula to study domain at 95% significant level.

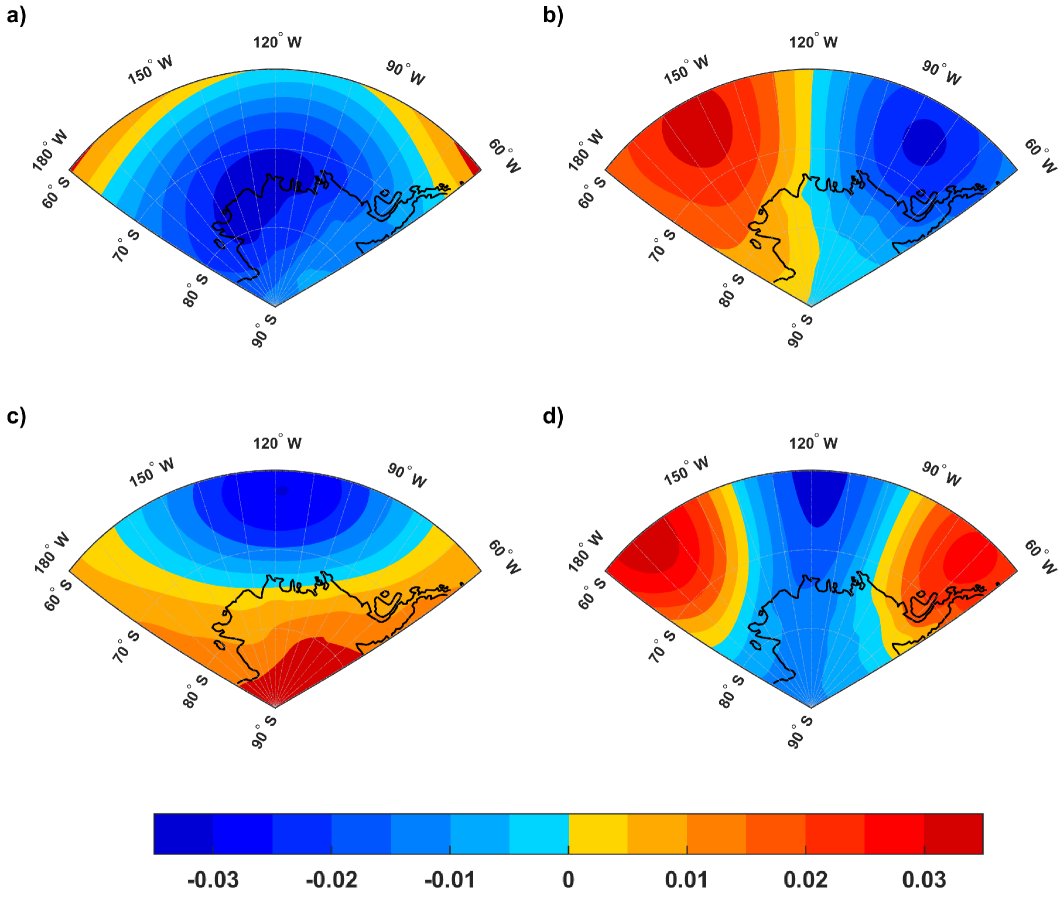

Figure 2. Spatial analysis of first four EOF modes (a,b,c and d) of daily geopotential height at 850 hpa over the region 60° S to 90°S and 180°W to 60°W.

Table S1). Given the strong correlation with precipitation over the rest of the domain, a similar frequency distribution and seasonal variability is expected over most of the WA domain. The rest of this section will focus on identifying the key drivers of EPEs at the two locations.

3.1 Dominant patterns of atmospheric variability over coastal WA

The dominant modes of near-surface atmospheric circulation over the study domain are identified from the EOF analysis of daily geopotential height anomalies at 850 hPa. The first dominant mode (EOF-1) which explains $\sim 48\%$ of the total variability is the Southern Annular Mode (SAM, Limpasuvan and Hartmann (1999); Thompson and Wallace (2000)). The spatial pattern is associated with an annular structure and a negative anomaly centred at 130°W (Figure-2a). The first PC time series shows a strong positive correlation (> 0.7) with SAM and it has a weak negative correlation with ASL- actual central pressure index (Supplementary Table S2).

The second EOF mode (EOF-2) (Figure-2b) explains $\sim 19\%$ variability. The spatial pattern is characterised by positive anomalies centred at 150°W (Amundsen Sea region in the western WA) and negative anomalies centred at 90°W (west of Antarctic Peninsula). This spatial pattern, consisting of pressure anomalies of opposite signs to the west of Antarctic Peninsula and over the Amundsen Sea region, is representative of the western branch of the

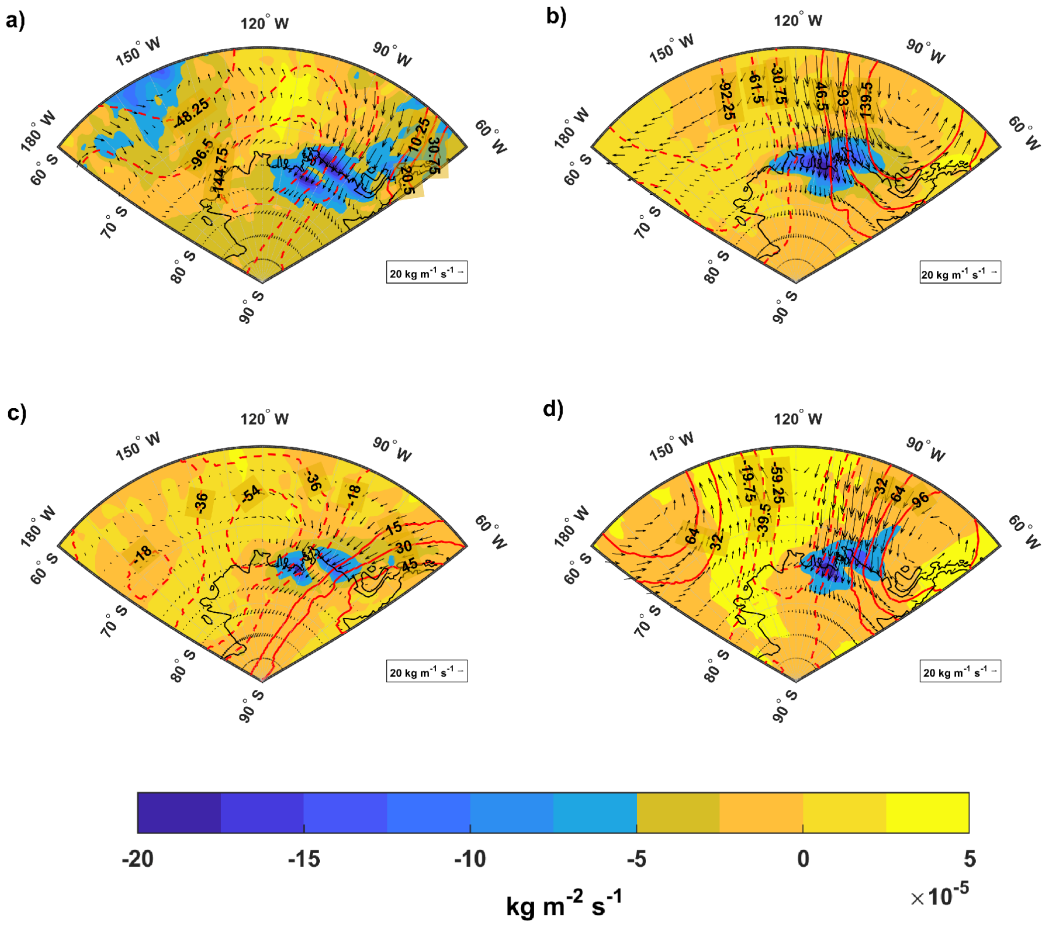

Figure 3. Composite anomalies of moisture divergence (shaded,in $kgm^{-2}s^{-1}$), moisture transport (vectors,in $kgm^{-1}s^{-1}$) and geopotential height at 850 hpa(positive and negative anomalies are represented by red solid lines and red dotted contours, respectively) during EPE days at EK, when only respective PC-1 (a), PC-2 (b), PC-3 (c) and PC-4 (d) modes are dominant.

PSA2 pattern. The change in polarity of this pattern (equivalent to a zonal shift in ASL) can be conveniently represented by the ASL lon index as presented in Deb et al. (2018). This is evident from a strong positive correlation (> 0.9) of the corresponding PC with ASL-lon index (Table S2).

The spatial pattern of EOF-3 mode (Figure-2c), which accounts for $\sim$ 17.14% of total variability, resembles the ENSO spatial pattern with positive (negative) anomalies over Amundsen Sea during El Niño (La Niña) events (Clem & Fogt, 2013; Deb et al., 2018). The modulation of this mode by eastern Pacific Ocean is further evident from a significant negative correlation (~ -0.5) of the PC time series with ENSO-ONI index (Table S2).

The EOF-4 mode explains around 8.04% of the total variability, and this is a structure that may be conducive for more 'atmospheric river' activity consisting of an elongated negative anomaly pattern extending from mid latitudes onto the continent (Figure-2d). The pattern, along with the blocking structures on either sides, shows close proximity to the observed atmospheric river pattern mentioned in Wille et al. (2019).

3.2 Role of the main atmospheric modes in driving EPEs over coastal WA

A particular atmospheric mode is considered to play the dominant role during an EPE day if the corresponding PC on that day shows the largest value among the 4 major modes. Composites of 3 important variables (e.g., divergence of moisture flux, moisture transport and geopotential height anomalies at 850 hPa) are computed during EPE days at EK dominated by each individual mode (Figure-3). For example, Figure-3a shows the composite for EPE days dominated by the first EOF mode. A cyclonic geopotential height anomaly is noticed over coastal WA which is consistent with the spatial pattern of EOF-1 mode in Figure-2a. A strong meridional moisture transport towards the continent leads to intense moisture convergence (magnitude $> 5{*}10^{-5}$ $kgm^{-2}s^{-1}$) along the eastern WA coastline (between 120°W and 60°W) and western Antarctic Peninsula (blue shading). This circulation anomaly explains the occurrence of EPEs at EK station during the days dominated by first mode of atmospheric variability over WA, i.e., the SAM.

Figure-3b shows that the EPE days at EK that are dominated by the second EOF mode show a dipole-like geopotential anomaly pattern with anti-cyclonic and cyclonic anomaly centres to the east (west) of $\sim$ 110°W. This pattern (which is clearly similar to spatial pattern of the second EOF mode) drives a strong meridional moisture transport towards the WA coast, with the strongest moisture convergence (magnitude $> 5{*}10^{-5}$ kg/m/s) concentrated over the ASE (140°W – 90°W).

Atmospheric circulation pattern during EPE days (at EK) dominated by the third EOF mode is shown in Figure-3c. Similar to the spatial pattern of EOF-3 (as shown in Figure-2c), a cyclonic circulation anomaly is observed over the Amundsen Sea region accompanied by anomalous moisture transport towards the coastal WA leading to intense moisture convergence along the coastline. However, the area of the strongest moisture convergence (i.e., magnitude$> 5{*}10^{-5}$ $kgm^{-2}s^{-1}$) is limited within the ASE (e.g., 100°W – 80°W longitude belt). Therefore, the cyclonic circulation anomaly associated with the third mode can bring large quantities of moisture towards the coastal stations over the ASE and cause EPEs.

EPE days at EK that are dominated by EOF-4 mode shows the most favourable pattern for producing atmospheric rivers (Figure-3d). This is further supported by composite of moisture transport anomalies during EPE days dominated by EOF-4 which shows a distinct band of moisture inflow from the mid-latitudes (Supplementary figure-S5b). This pattern is associated with strong moisture transport towards the coastal WA and leads to intense moisture convergence with particularly large values (magnitude $> 5{*}10^{-5}$ $kgm^{-2}s^{-1}$) concentrated over the ASE (110°W – 80°W longitude belt).

Similarly, the composite anomalies during EPE days at BP when dominated by 4 individual EOF modes (Supplementary figure-S3) are broadly similar to that in the case of EK (i.e., Figure-3), particularly for EOF-2 and EOF-4. However, the anomaly centres corresponding to EOF-1 and EOF-3 are slightly shifted to the west when compared to Figure-3. Also, the spatial extent and magnitude of moisture convergence is less when compared to that of EK (Figure-3). Overall, the magnitude of precipitation associated with EOF-2 mode (ASL-lon) and EOF-4 mode (suspected atmospheric rivers) is larger by at least 2 mm/day over ASE compared to other modes (Supplementary figure-S4).

3.3 Relative seasonal contribution of different atmospheric modes

Figure-4a and 4b indicates the seasonal contribution of EOFs to EPEs at the two coastal locations over WA while the 'total' contribution of the EOF modes is shown in Figure-4c and d. The second EOF mode or the ASL-lon zonal pattern (i.e., the coupling of ASL with a blocking high over the Antarctic Peninsula) was found to be the leading driver of EPEs over coastal WA with a total contribution of 40.28% (49.23 %) at EK (BP) (Figure-4c and 4d). This pattern was previously reported to be the main driver of high snowfall events over

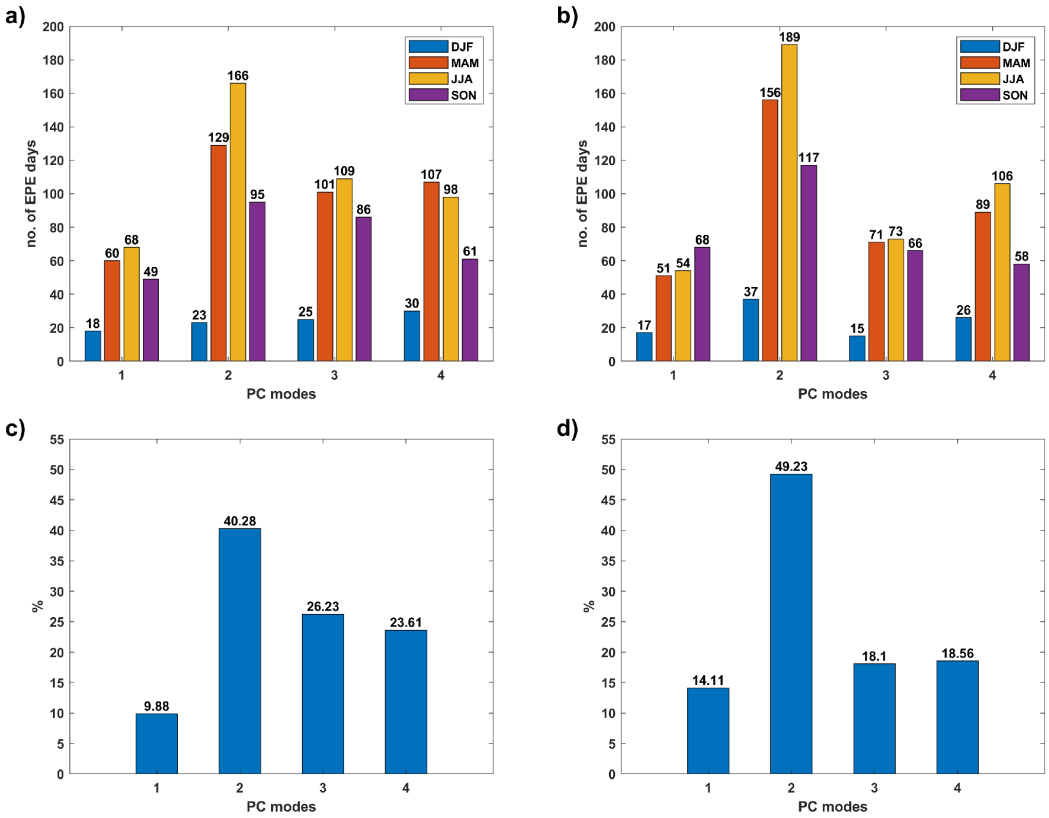

Figure 4. Seasonal distribution of EPE days occurring with respective PCs at (a) EK and (b) BP. Total contribution of dominant PCs to EPEs of (c) EK and (d) BP during the period 1979-2016.

Thwaites Glacier region of WA (Maclennan & Lenaerts, 2021). The pattern is particularly important for EPEs during MAM, JJA and SON seasons (Figure-4a and 4b). This is followed by EOF-3 (representative of ENSO influence over WA) and EOF-4 (suspected to be linked to the intrusion of atmospheric rivers) modes with percentage contributions of 26.23 and 23.61, respectively, to EPE days at EK (Figure-4c). Their respective contribution is 18.1 % and 18.56 % at BP (Figure-4d). On average, EOF-4 is slightly more dominant than EOF-3 during DJF, MAM and JJA seasons while EOF-3 is more dominant in SON (Figure-4a and 4b). In contrast, the first EOF mode associated with SAM showed the least percentage contribution to EPE days in all four seasons. The total contribution of EOF-1 to EPE days is 9.88 % and 14.11 % at EK and BP, respectively.

4 Discussion and Conclusions

Despite several attempts to understand the seasonal and inter annual changes in mass balance and precipitation over WA, only a few studies have attempted to understand the short lived extreme precipitation events and their atmospheric drivers. Most of annual precipitation over the coastal WA comes from EPEs (Turner et al., 2019). For example, we find that at two coastal stations over the ASE of WA (EK and BP), EPEs at EK and BP contributes around 41% of the total precipitation, with the maximum contribution from EPEs noted in JJA followed by MAM, SON and DJF seasons. As EK and BP are representative of the precipitation over the coastal WA, and also over inland areas (as evident from the significantly high correlation in Figure-1e and 1f), precipitation from these two stations are used to understand the frequency distribution and drivers of EPEs over coastal WA, and particularly the ASE.

The 'ASL-lon' pattern or the zonally coupled structure consisting of ASL and a blocking high over the Antarctic Peninsula was found to be the leading driver of EPEs over the ASE. Total contribution from 'ASL-lon' pattern to EPEs at the coastal stations over the ASE ($\sim 40-49\%$) is significantly higher than the total contribution from PSA-1 pattern ($\sim 18-26\%$) and the atmospheric river pattern ($\sim 18-24\%$) (Figure-4c and 4d). The 'ASL-lon' pattern was previously shown to be responsible for high snowfall events over Thwaites Glacier region of WA in a previous study (Maclennan & Lenaerts, 2021). ASL-lon pattern shows the maximum (minimum) contribution to EPEs in JJA (DJF).This seasonality in the contribution of ASL-lon is due to the well-defined annual cycle in the zonal location of ASL with a clear westward movement towards the Ross Sea in JJA which drives strong northerly wind into the ASE (J. S. Hosking et al., 2013; M. N. Raphael et al., 2016).

El Niño years associated with a large positive geopotential height anomaly centre off the coast of WA which drives anomalous warm and moist air advection into the WA ice sheet (Welhouse et al., 2016; Deb et al., 2018). The local circulation changes during El Niño years are associated with an increased likelihood of extreme surface temperature (Deb et al., 2018), and an increase in precipitation over the ASE (Paolo et al., 2018; Zhang et al., 2021). The ENSO signal over WA is captured by EOF-3 mode in our study, and explains more then 25% of the EPEs over coastal WA.

In our analysis, EOF-4 mode (suspected AR pattern) explains only 8% of the total variability, but it is associated with the most intense moisture convergence among all the modes (Figure-4). Despite their extreme rarity, atmospheric rivers have been linked to a number of heavy precipitation events across Antarctica (Gorodetskaya et al., 2014; Wille et al., 2019; Adusumilli et al., 2021). Our analysis shows that during the simulation period of 1979-2016, PC-4 mode is associated with approximately 18-23% of the extreme snowfall days over ASE (Figure-4c and 4d). However, their contribution in terms of the actual amount of snowfall will be much higher as the EPEs during PC-4 mode are much more intense (Supplementary figure-S4) due to the high moisture convergence.

As a large fraction of the precipitation over coastal WA comes from EPEs, the future mass balance changes over WA will be highly sensitive to the future changes in the atmospheric drivers of EPEs identified in this study. A westward (and poleward) shift of ASL (J. S. Hosking et al., 2016; Brown et al., 2020) along with a likely increase in the frequency of atmospheric rivers land falling on Antarctica by the end of the 21^{st} century (Espinoza et al., 2018; Payne et al., 2021) are expected to make a positive contribution to future mass balance changes over WA. However, projected change in ENSO, and hence the associated teleconnection, remain highly uncertain. Therefore, it is essential that the dynamics of these drivers and their interaction with the WA coastline are well-understood in order to constrain the future mass balance changes over ASE and coastal WA.

5 Open Research

Data availability statement

All the datasets for this research are openly available online.
RACMO version 3p2 limited area atmospheric model precipitation data used in this study is available online through British Antarctic Survey repository : `https://doi.org/10.5285/bbf12a6f-7d97-4951-9bd1-e4224e2abac9`
ERA-Interim data is available at European Centre for Medium-Range Weather Forecasts (ECMWF) : `https://apps.ecmwf.int/datasets/`
ENSO Oceanic Niño Index (ONI) is obtainable from National Weather Service, Climate Prediction Center : `https://origin.cpc.ncep.noaa.gov/products/analysis_monitoring/ensostuff/ONI_v5.php`
Marshall Southern Annular Mode (SAM) index available at : `http://www.nerc-bas.ac.uk/icd/gjma/sam.html`
Amundsen Sea Low (ASL) index available at : `http://scotthosking.com/asl_index`

Acknowledgments

Both the authors were funded by the Indian Institute of Technology Kharagpur and the Ministry of Education, Govt. of India. We also acknowledge the support of the National Centre for Polar and Ocean Research, Goa (project: NCPOR/2019/PACER-POP/AS-02).

References

Adusumilli, S., A Fish, M., Fricker, H. A., & Medley, B. (2021). Atmospheric river precipitation contributed to rapid increases in surface height of the west antarctic ice sheet in 2019. *Geophysical Research Letters*, *48*(5), e2020GL091076.

Banta, J. R., McConnell, J. R., Frey, M. M., Bales, R. C., & Taylor, K. (2008). Spatial and temporal variability in snow accumulation at the west antarctic ice sheet divide over recent centuries. *Journal of Geophysical Research: Atmospheres*, *113*(D23).

Brown, J. R., Brierley, C. M., An, S.-I., Guarino, M.-V., Stevenson, S., Williams, C. J., ... others (2020). Comparison of past and future simulations of enso in cmip5/pmip3 and cmip6/pmip4 models. *Climate of the Past*, *16*(5), 1777–1805.

Clem, K. R., & Fogt, R. L. (2013). Varying roles of enso and sam on the antarctic peninsula climate in austral spring. *Journal of Geophysical Research: Atmospheres*, *118*(20), 11–481.

Clem, K. R., & Fogt, R. L. (2015). South pacific circulation changes and their connection to the tropics and regional antarctic warming in austral spring, 1979–2012. *Journal of Geophysical Research: Atmospheres*, *120*(7), 2773–2792.

Deb, P., Orr, A., Bromwich, D. H., Nicolas, J. P., Turner, J., & Hosking, J. S. (2018). Summer drivers of atmospheric variability affecting ice shelf thinning in the amundsen sea embayment, west antarctica. *Geophysical Research Letters*, *45*(9), 4124–4133.

Deb, P., Orr, A., Hosking, J. S., Phillips, T., Turner, J., Bannister, D., ... Colwell, S. (2016). An assessment of the polar weather research and forecasting (wrf) model representation of near-surface meteorological variables over west antarctica. *Journal of Geophysical Research: Atmospheres*, *121*(4), 1532–1548.

Dee, D. P., Uppala, S. M., Simmons, A. J., Berrisford, P., Poli, P., Kobayashi, S., ... others (2011). The era-interim reanalysis: Configuration and performance of the data assimilation system. *Quarterly Journal of the royal meteorological society*, *137*(656), 553–597.

Déry, S. J., & Yau, M. (1999). A bulk blowing snow model. *Boundary-Layer Meteorology*, *93*(2), 237–251.

Espinoza, V., Waliser, D. E., Guan, B., Lavers, D. A., & Ralph, F. M. (2018). Global analysis of climate change projection effects on atmospheric rivers. *Geophysical Research Letters*, *45*(9), 4299–4308.

Ettema, J., Van den Broeke, M., Van Meijgaard, E., Van de Berg, W., Box, J., & Steffen, K. (2010). Climate of the greenland ice sheet using a high-resolution climate model–part 1: Evaluation. *The Cryosphere*, *4*(4), 511–527.

Ghil, M., & Mo, K. (1991). Intraseasonal oscillations in the global atmosphere. part ii: Southern hemisphere. *Journal of Atmospheric Sciences*, *48*(5), 780–790.

Giorgi, F., Shields Brodeur, C., & Bates, G. T. (1994). Regional climate change scenarios over the united states produced with a nested regional climate model. *Journal of Climate*, *7*(3), 375–399.

Gorodetskaya, I. V., Tsukernik, M., Claes, K., Ralph, M. F., Neff, W. D., & Van Lipzig, N. P. (2014). The role of atmospheric rivers in anomalous snow accumulation in east antarctica. *Geophysical Research Letters*, *41*(17), 6199–6206.

Hosking, J. S., Orr, A., Bracegirdle, T. J., & Turner, J. (2016). Future circulation changes off west antarctica: Sensitivity of the amundsen sea low to projected anthropogenic forcing. *Geophysical Research Letters*, *43*(1), 367–376.

Hosking, J. S., Orr, A., Marshall, G. J., Turner, J., & Phillips, T. (2013). The influence of the amundsen–bellingshausen seas low on the climate of west antarctica and its representation in coupled climate model simulations. *Journal of Climate*, *26*(17), 6633–6648.

Hosking, S. (2020). *The climate data guide: Amundsen sea low indices, edited by: National center for atmospheric research staff.* Retrieved from `https://climatedataguide.ucar.edu/climate-data/amundsen-sea-low-indices`

Irving, D., & Simmonds, I. (2015). A novel approach to diagnosing southern hemisphere planetary wave activity and its influence on regional climate variability. *Journal of Climate*, *28*(23), 9041–9057.

Kidson, J. W. (1988). Interannual variations in the southern hemisphere circulation. *Journal of Climate*, *1*(12), 1177–1198.

Kuipers Munneke, P., Van den Broeke, M., Lenaerts, J., Flanner, M., Gardner, A., & Van de Berg, W. (2011). A new albedo parameterization for use in climate models over the antarctic ice sheet. *Journal of Geophysical Research: Atmospheres*, *116*(D5).

Lau, K., Sheu, P., & Kang, I.-S. (1994). Multiscale low-frequency circulation modes in the global atmosphere. *Journal of the Atmospheric Sciences*, *51*(9), 1169–1193.

Lenaerts, J., Van den Broeke, M., Déry, S., König-Langlo, G., Ettema, J., & Munneke, P. K. (2010). Modelling snowdrift sublimation on an antarctic ice shelf. *The Cryosphere*, *4*(2), 179–190.

Lenaerts, J. T., van Meijgaard, E., van den Broeke, M. R., Ligtenberg, S. R., Horwath, M., & Isaksson, E. (2013). Recent snowfall anomalies in dronning maud land, east antarctica, in a historical and future climate perspective. *Geophysical Research Letters*, *40*(11), 2684–2688.

Limpasuvan, V., & Hartmann, D. L. (1999). Eddies and the annular modes of climate variability. *Geophysical Research Letters*, *26*(20), 3133–3136.

Maclennan, M. L., & Lenaerts, J. T. (2021). Large-scale atmospheric drivers of snowfall over thwaites glacier, antarctica. *Geophysical Research Letters*, *48*(17), e2021GL093644.

Marshall, G. (2018). *The climate data guide: Marshall southern annular mode (sam) index (station-based), edited by: National center for atmospheric research staff.*

Marshall, G. J., Thompson, D. W., & van den Broeke, M. R. (2017). The signature of southern hemisphere atmospheric circulation patterns in antarctic precipitation. *Geophysical Research Letters*, *44*(22), 11–580.

Mayewski, P. A., Meredith, M., Summerhayes, C., Turner, J., Worby, A., Barrett, P., ... others (2009). State of the antarctic and southern ocean climate system. *Reviews of Geophysics*, *47*(1).

Mo, K. C., & Paegle, J. N. (2001). The pacific–south american modes and their downstream effects. *International Journal of Climatology: A Journal of the Royal Meteorological Society*, *21*(10), 1211–1229.

Noone, D., & Simmonds, I. (1998). Implications for the interpretation of ice-core isotope data from analysis of modelled antarctic precipitation. *Annals of Glaciology*, *27*, 398–402.

Orr, A., Phillips, T., Webster, S., Elvidge, A., Weeks, M., Hosking, S., & Turner, J. (2014). Met office unified model high-resolution simulations of a strong wind event in antarctica. *Quarterly Journal of the Royal Meteorological Society*, *140*(684), 2287–2297.

Paolo, F., Padman, L., Fricker, H., Adusumilli, S., Howard, S., & Siegfried, M. (2018). Response of pacific-sector antarctic ice shelves to the el niño/southern oscillation. *Nature geoscience*, *11*(2), 121–126.

Payne, A. J., Nowicki, S., Abe-Ouchi, A., Agosta, C., Alexander, P., Albrecht, T., ... others (2021). Future sea level change under coupled model intercomparison project phase 5 and phase 6 scenarios from the greenland and antarctic ice sheets. *Geophysical Research Letters*, *48*(16), e2020GL091741.

Pritchard, H., Ligtenberg, S. R., Fricker, H. A., Vaughan, D. G., van den Broeke, M. R., & Padman, L. (2012). Antarctic ice-sheet loss driven by basal melting of ice shelves. *Nature*, *484*(7395), 502–505.

Pritchard, H. D., Arthern, R. J., Vaughan, D. G., & Edwards, L. A. (2009). Extensive dynamic thinning on the margins of the greenland and antarctic ice sheets. *Nature*, *461*(7266), 971–975.

Raphael, M. (2004). A zonal wave 3 index for the southern hemisphere. *Geophysical Research Letters*, *31*(23).

Raphael, M. N., Marshall, G., Turner, J., Fogt, R., Schneider, D., Dixon, D., ... Hobbs, W. R. (2016). The amundsen sea low: variability, change, and impact on antarctic climate. *Bulletin of the American Meteorological Society*, *97*(1), 111–121.

Rignot, E., Bamber, J. L., Van Den Broeke, M. R., Davis, C., Li, Y., Van De Berg, W. J., & Van Meijgaard, E. (2008). Recent antarctic ice mass loss from radar interferometry and regional climate modelling. *Nature geoscience*, *1*(2), 106–110.

Rignot, E., Mouginot, J., Scheuchl, B., Van Den Broeke, M., Van Wessem, M. J., & Morlighem, M. (2019). Four decades of antarctic ice sheet mass balance from 1979–2017. *Proceedings of the National Academy of Sciences*, *116*(4), 1095–1103.

Sodemann, H., & Stohl, A. (2009). Asymmetries in the moisture origin of antarctic precipitation. *Geophysical research letters*, *36*(22).

Summerhayes, C., Ainley, D., Barrett, P., Bindschadler, R., Clarke, A., Convey, P., ... others (2009). The antarctic environment in the global system. *Antarctic climate change and the environment. Scientific Committee on Antarctic Research, Cambridge*, 1–32.

Thompson, D. W., & Wallace, J. M. (2000). Annular modes in the extratropical circulation. part i: Month-to-month variability. *Journal of climate*, *13*(5), 1000–1016.

Turner, J., Bindschadler, R., Convey, P., Di Prisco, G., Fahrbach, E., Gutt, J., ... Summerhayes, C. (2009). *Antarctic climate change and the environment.*

Turner, J., Phillips, T., Thamban, M., Rahaman, W., Marshall, G. J., Wille, J. D., ... others (2019). The dominant role of extreme precipitation events in antarctic snowfall variability. *Geophysical Research Letters*, *46*(6), 3502–3511.

Undén, P., Rontu, L., Järvinen, H., Lynch, P., Calvo, J., Cats, G., ... others (2002). Hirlam-5 scientific documentation.

Van Wessem, J., Reijmer, C., Morlighem, M., Mouginot, J., Rignot, E., Medley, B., ... others (2014). Improved representation of east antarctic surface mass balance in a regional atmospheric climate model. *Journal of Glaciology*, *60*(222), 761–770.

Vaughan, D. G., Marshall, G. J., Connolley, W. M., King, J. C., & Mulvaney, R. (2001). Devil in the detail. *Science*, *293*(5536), 1777–1779.

Welhouse, L. J., Lazzara, M. A., Keller, L. M., Tripoli, G. J., & Hitchman, M. H. (2016). Composite analysis of the effects of enso events on antarctica. *Journal of Climate*, *29*(5), 1797–1808.

Wille, J. D., Favier, V., Dufour, A., Gorodetskaya, I. V., Turner, J., Agosta, C., & Codron, F. (2019). West antarctic surface melt triggered by atmospheric rivers. *Nature Geoscience*, *12*(11), 911–916.

Zhang, B., Yao, Y., Liu, L., & Yang, Y. (2021). Interannual ice mass variations over the antarctic ice sheet from 2003 to 2017 were linked to el niño-southern oscillation. *Earth and Planetary Science Letters*, *560*, 116796.

Zhu, Y., & Newell, R. E. (1998). A proposed algorithm for moisture fluxes from atmospheric rivers. *Monthly weather review*, *126*(3), 725–735.

Zwally, H. J., Robbins, J. W., & Luthcke, S. B. (2017). Mass balance of east antarctic ice sheet: Reconciling icesat altimetry with grace gravimetry and long-term ice history. In *Agu fall meeting abstracts* (Vol. 2017, pp. C23D–08).

[Geophysical Research Letters]

Supporting Information for

[Relative contribution of atmospheric drivers to 'extreme' snowfall over the Amundsen Sea Embayment]

[Sai Prabala Swetha Chittella[1], Pranab Deb[2], Jan Melchior van Wessem[3]]

[[1,2]Centre for Oceans, Rivers, Atmosphere and Land Sciences, Indian Institute of Technology Kharagpur

[3]Institute for Marine and Atmospheric Research Utrecht, Utrecht University, Utrecht, the Netherlands]

Contents of this file

Introduction

This supporting information provides the figures for: (1) seasonal frequency distribution for both Evans Knoll (EK) and Bear Peninsula (BP) station, (2) composites of divergence of moisture flux, moisture transport and geopotential height anomalies at 850hpa during EPE days at BP station dominated by each individual mode (same as Figure-3 in main article, but for BP), (3) composites of precipitation anomalies for days corresponding to 4 individual PC modes, (4) composite of moisture transport anomalies of PC-2 and PC-4 modes for EK and BP, (5) a table containing number of EPEs per season at both locations EK and BP and (6) a table containing correlation between PC modes and several Climate indices such as ENSO, SAM and ASL-Ion.

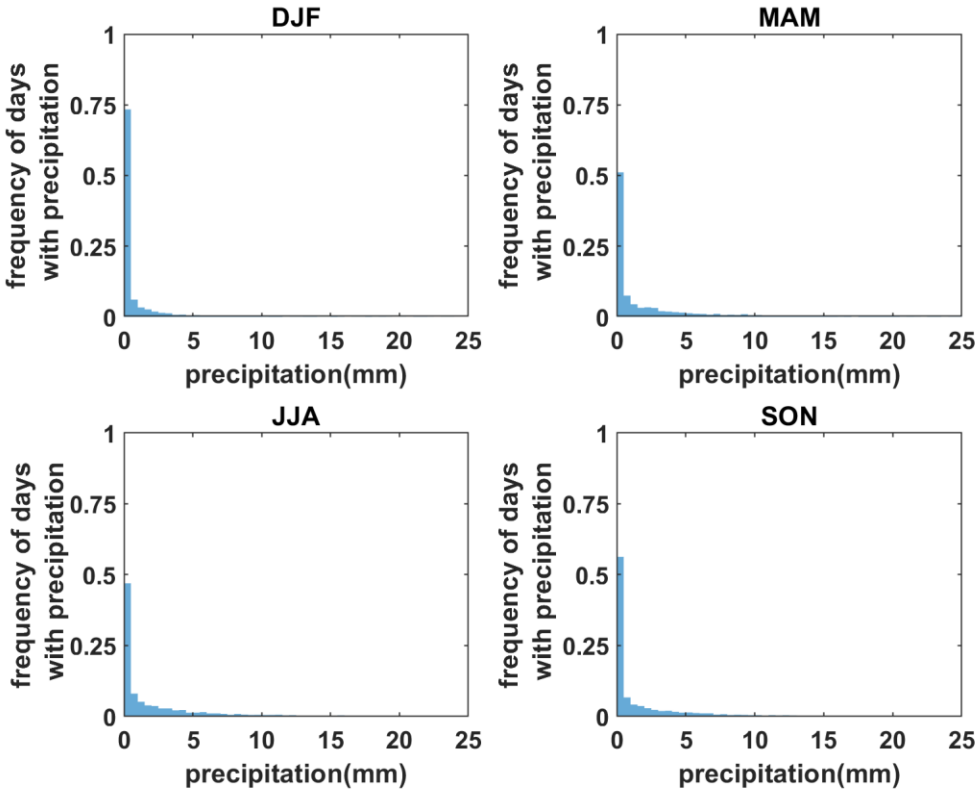

Figure S1. Seasonal frequency distribution of daily precipitation at Evans Knoll during 1979 to 2016

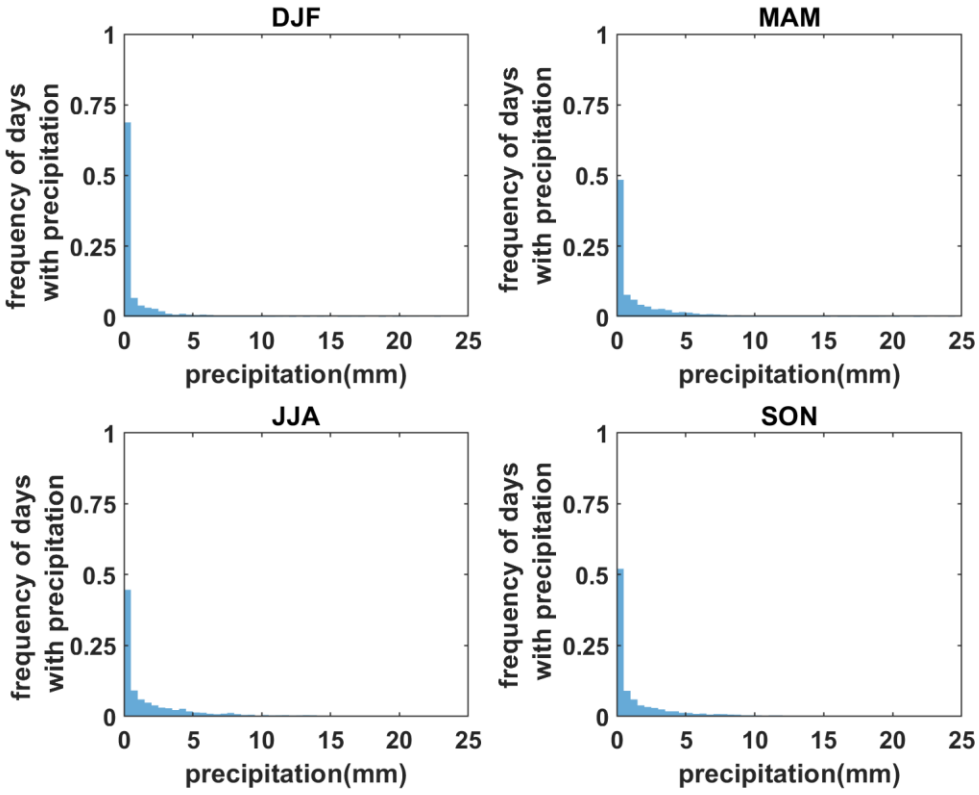

Figure S2. Seasonal frequency distribution of daily precipitation at Bear Peninsula during 1979 to 2016

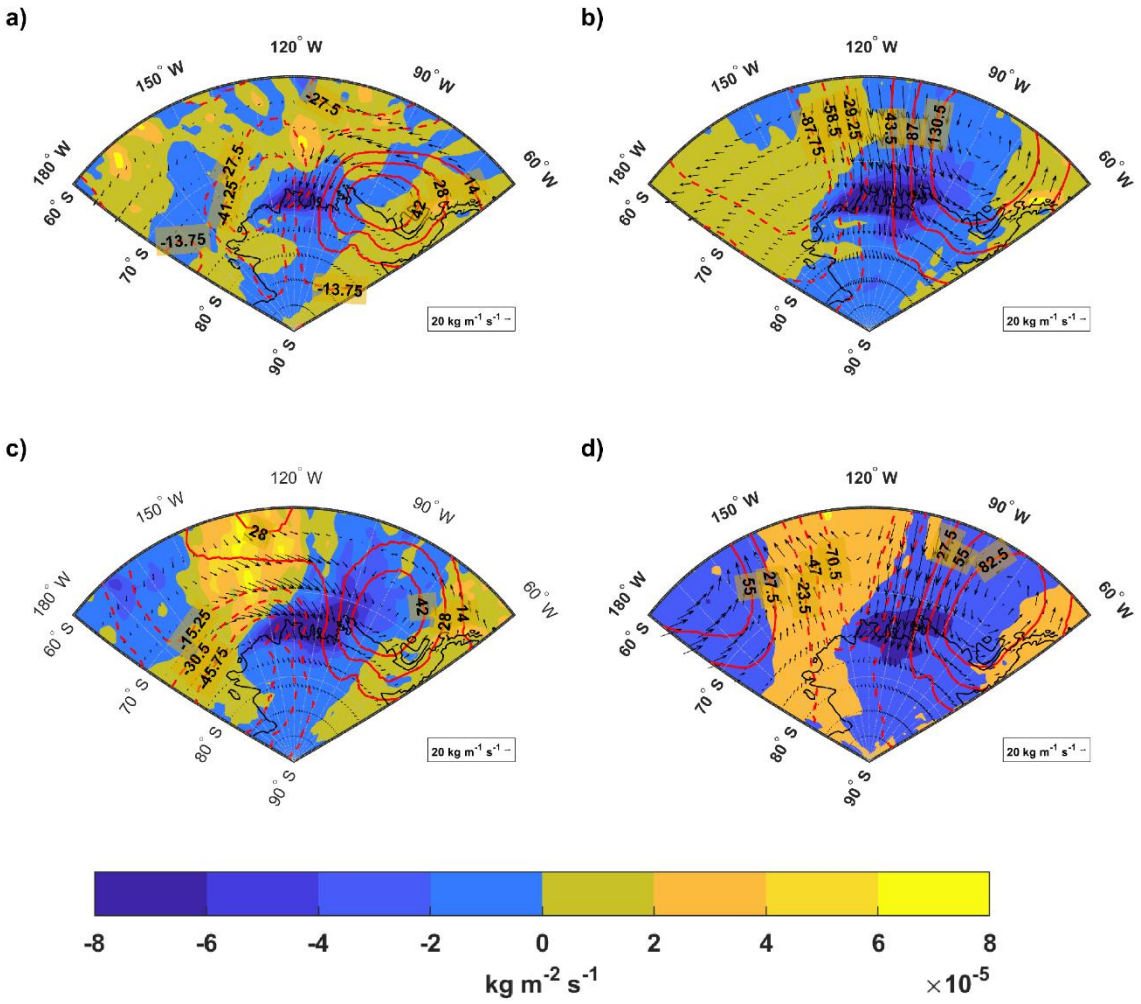

Figure S3. Composite anomalies of moisture divergence (shaded, $kgm^{-2}s^{-1}$), moisture transport (vectors, $kgm^{-1}s^{-1}$) and geopotential height at 850 hpa (positive and negative anomalies are represented by red solid lines and red dotted lines) during EPE days of BP, when only respective PC-1 (a), PC-2 (b), PC-3 (c) and PC-4 (d) modes are dominant.

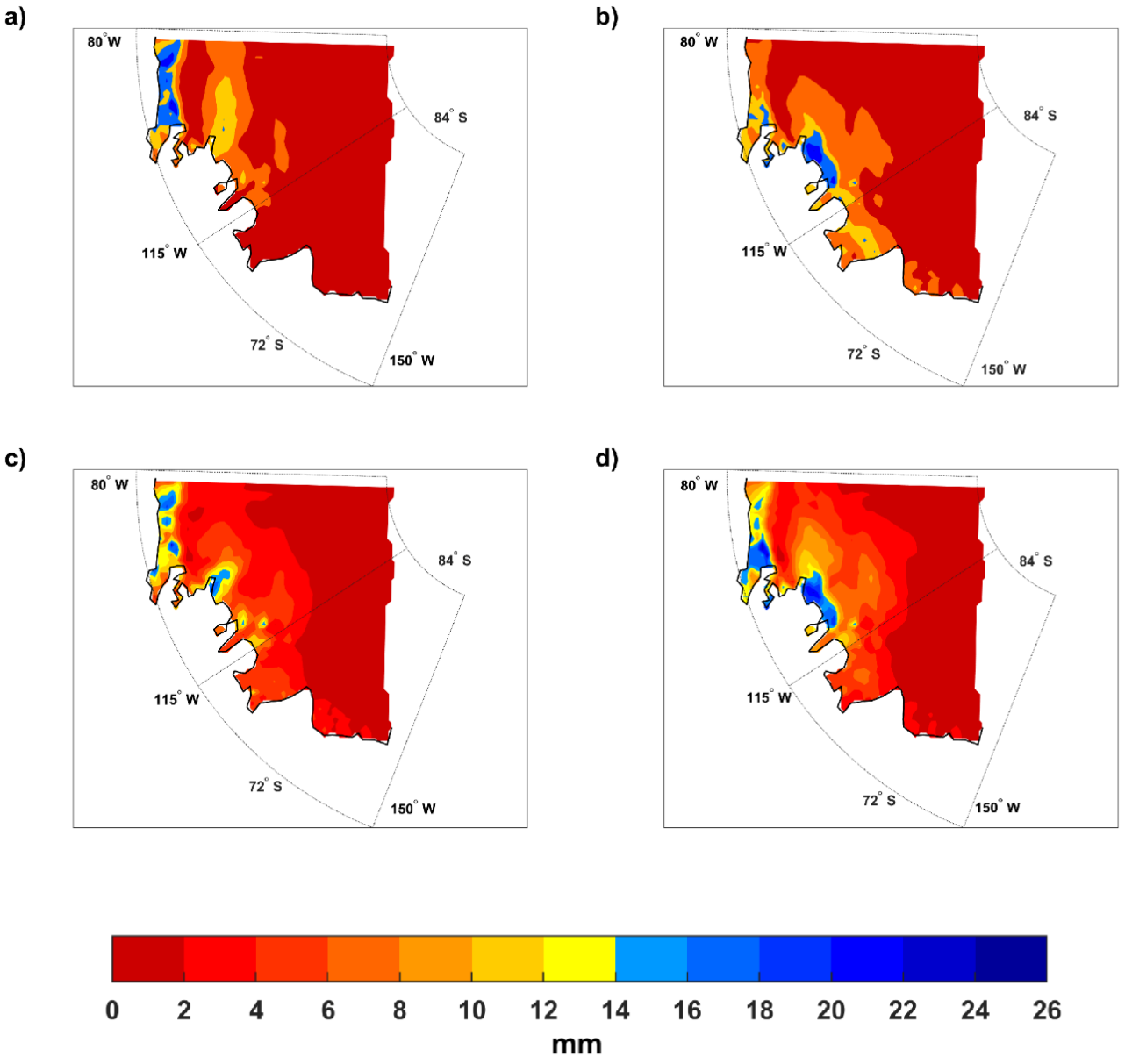

Figure S4. Composite of precipitation anomalies (mm) during EPE days at EK, when only respective PC-1 (a), PC-2 (b), PC-3 (c), PC-4 (d) modes are dominant.

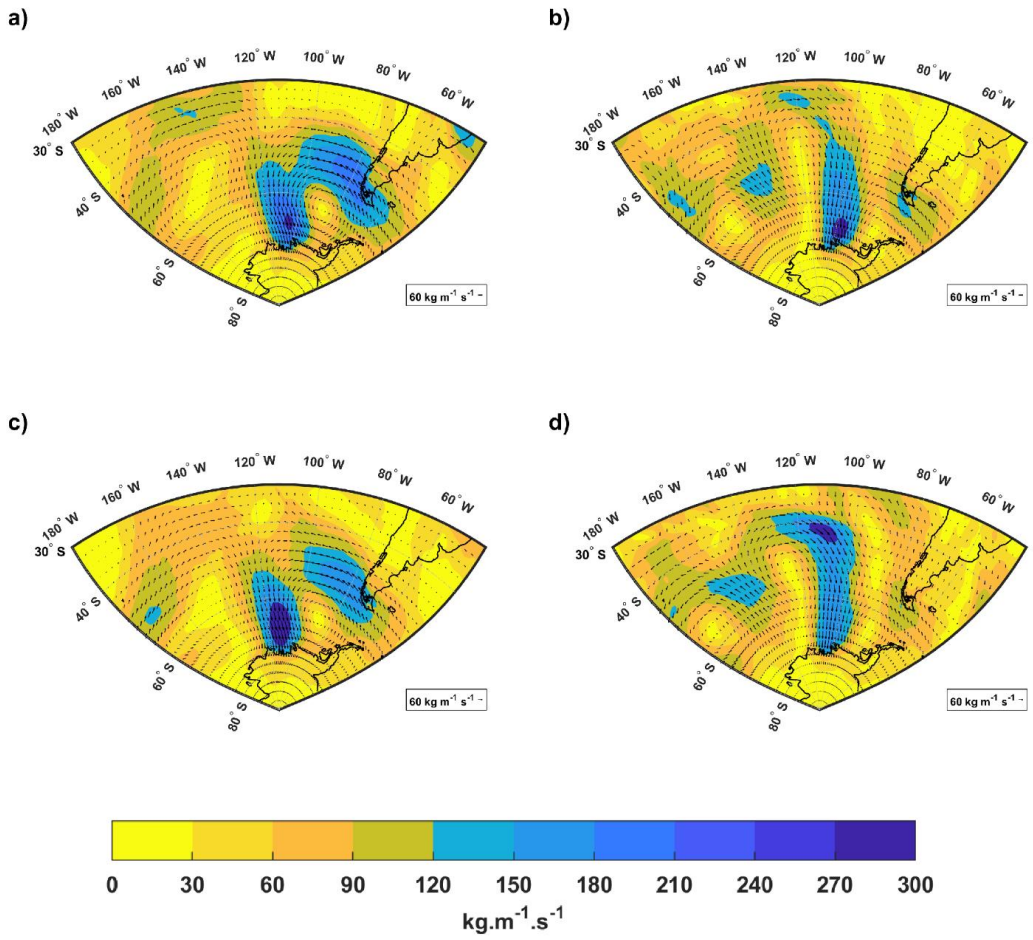

Figure S5. Composite of moisture transport anomalies ($kgm^{-1}s^{-1}$) during EPE days at EK, when only respective PC-2 (a) and PC-4 (b) modes are dominant. Composite anomalies of moisture transport ($kgm^{-1}s^{-1}$) during EPE days at BP, when only respective PC-2 (c) and PC-4 (d) modes are dominant.

Seasons/Stations	Evans Knoll (EK)	Bear Peninsula (BP)
DJF	**54**	**62**
MAM	231	223
JJA	**244**	**233**
SON	164	176

Table S1. Total number of EPEs obtained for all seasons at EK and BP for time period 1979-2016.

Climate index	season	PC1	PC2	PC3	PC4
ENSO-ONI	**DJF**	-0.38	-0.07	**-0.32**	-0.28
ENSO-ONI	**MAM**	-0.07	-0.10	**-0.40**	-0.10
ENSO-ONI	**JJA**	-0.07	0.14	**-0.50**	-0.04
ENSO-ONI	**SON**	-0.25	-0.25	**-0.56**	0.32
SAM	**DJF**	-0.03	-0.14	-0.05	-0.16
SAM	**MAM**	**0.84**	0.37	-0.03	-0.35
SAM	**JJA**	**0.73**	0.11	-0.01	-0.16
SAM	**SON**	**0.90**	0.14	0.14	-0.01
ASL	**DJF**	**-0.45**	-0.02	0.14	-0.11
ASL	**MAM**	**-0.38**	0.12	-0.15	-0.12
ASL	**JJA**	**-0.46**	-0.14	0.04	0.06
ASL	**SON**	**-0.30**	-0.08	-0.15	-0.26
ASL-lon	**DJF**	-0.09	**0.94**	0.05	-0.08
ASL-lon	**MAM**	0.46	**0.96**	0.07	-0.41
ASL-lon	**JJA**	0.38	**0.95**	0.09	-0.19
ASL-lon	**SON**	0.35	**0.96**	0.15	-0.06

Table S2. Seasonal correlation between PC modes and climate indices such as ENSO-ONI, SAM, ASL, ASL-lon indices.